IEEE Access
Multidisciplinary | Rapid Review | Open Access Journal

Received June 15, 2021, accepted July 3, 2021, date of publication July 8, 2021, date of current version July 19, 2021.

Digital Object Identifier 10.1109/ACCESS.2021.3095665

Torque Ripple Reduction of PMSM With Small Capacitor Drive Systems Based on Combined Control Method

CHAO ZHANG, (Member, IEEE), LEI XU, (Member, IEEE), XIAOYONG ZHU, (Member, IEEE), YI DU, (Member, IEEE), AND LI QUAN

School of Electrical and Information Engineering, Jiangsu University, Zhenjiang 212013, China
Jiangsu Key Laboratory of Drive and Intelligent Control for Electric Vehicle, Jiangsu University, Zhenjiang 212013, China

Corresponding author: Xiaoyong Zhu (zxyff@ujs.edu.cn)

This work was supported by the National Natural Science Foundation of China under Grant 52077098 and Grant 51907081.

ABSTRACT Small capacitor motor drive systems have received increased attention due to higher reliability and longer lifespan. However, small capacitor motor drive systems suffer from poor dynamic performance and larger torque ripple. In this paper, a combined control method is presents to improve the performance of small capacitor motor drive systems. On the one hand, this combined control strategy adopts injected harmonic current to reduce the fluctuation voltage on the DC-link, which provide better conditions for high-performance operation of permanent magnet synchronous motor. To satisfy the harmonic standard of IEC61000-3-2, the guideline of injected harmonic current is deduced according to motor power and the input power factor. On the other hand, an improved repetitive control in parallel with PI control is applied into motor control to effectively suppress motor torque ripple under the condition of the periodic pulsation voltage on the DC-link. In addition, this control method has good dynamic motor performance. Experiments are conducted, and the results verify the feasibility and effectiveness of the combined control strategy.

INDEX TERMS Fluctuation voltage, injected harmonic current, repetitive control, small capacitor motor drive.

I. INTRODUCTION

Nowadays, motor drive systems have been widely applied in industrial production and home application. For existing motor drive systems powered by the grid, a bulky electrolytic capacitor is used to absorb the grid pulsating power to keep the DC-link voltage stable, which is the basis for high motor performance [1], [2]. However, as the electrolyte evaporates, electrolytic capacitors have problems such as reduced capacity, increased equivalent resistance, and poor lifespan. In fact, electrolytic capacitors are the least reliable components in drive systems, and 60% of the failures of drive systems is caused by electrolytic capacitors [3].

Compared with electrolytic capacitors, film capacitors have higher reliability, and longer lifespan. Thus, when electrolytic capacitors are replaced by film capacitors, motor drive systems significantly reduce failure rate [4]. However, due to cost constraints, small film capacitors in the motor drive system are only 5-10% of the electrolytic capacitor, which is called small capacitance (SC) motor drive systems. However, SC motor drive systems suffers from high torque ripple, lower grid quality and lower efficiency due to the reduction of the DC-link capacitor [5].

SC motor drive systems based on active power decoupling converters can significantly improve the grid quality and the motor performance [6], [7]. However, these systems have high cost due to added power switches and passive components, which are not applied in low-cost applications, such as air conditioner, refrigerator, and washing machine. In contrast, SC motor drive systems based on modified control method are more popular in these low-cost applications. However, there is serious voltage fluctuation on the DC-link because only one small film capacitor is used to buffer the grid pulsating power, which degrades the quality of the gird current and increase the motor torque ripple. In addition, SC motor drive systems based on modified control method exhibit weak damping characteristics, which result in this type drive systems have poor resistance to external

The associate editor coordinating the review of this manuscript and approving it for publication was Tariq Masood.

disturbances [8]. But, the advantages of the high density and low cost still attract a large number of people to study.

Presently, the research topics of SC drive systems based on modified control method mainly focuses on how to improve grid quality or how to realize stable operation under external disturbance conditions. In theory, higher input power factor (PF) can be achieved by adjusting the motor power even without PFC circuits, and there are some efforts to improve the input PF [9]. A power loop connected in series between the motor speed loop and the current loop has been extensively studied. According to the characteristics of grid power pulsation, resonance control and fuzzy control are applied in inverter output power control to improve the input PF of SC motor drive systems [10]–[12]. However, SC motor drive system have higher THD of the grid current under these control methods.

Recently, some THD reduction methods for SC motor drive systems have been widely investigated [13]. Similar to control methods of input PF, the THD of SC motor drive system can also be reduced by controlling the motor phase current [12]. In [14], the relationship between the grid current and motor phase current is analyzed, and the THD of motor phase current is controlled to suppress the THD of SC motor drive systems according to instantaneous power theory. In [15], the fluctuation of DC-link voltage is limited to a given range, which can also reduce the THD of the motor phase current. In [16], the d-axis axis or q-axis reference current is calculated according the relationship between the grid current and the fluctuation of DC-link voltage. However, motors need to participate in power decoupling in these applications. Thus, motors suffer from the degradation of system performances, such as discontinuities motor phase currents, low efficiency and larger torque ripple.

In addition, when the load is constant, motor drive systems exhibit negative impedance characteristics [17]–[19]. For this type of SC motor drive systems, grid input power and motor output power are tightly coupled. These two characteristics degrades the stability of SC motor drive systems. Thus, how to implement stable operation is another research hotspot for SC motor drive systems. Passive damping circuits can increase the stability of SC motor drive systems. However, these circuits also increase cost and physical size of drive systems. To deal with these issues, virtual damping capacitor is introduced to increase the DC-link capacitor in [20]. In [21], the motor inverter is used to control the damping current of DC-link capacitor by adjusting the inverter output voltage, which is called virtual damping resistor. In [9], [22], [23], the torque-producing reference current is modified according the characteristic of DC-bus voltage or grid power, which dynamically changes the impedance of the load. In these methods, the negative impedance of the motor drive system is converted into positive damping characteristics, and improve the stability of the SC motor drive system.

Although the above-mentioned control methods are effective for improving the performance of SC motor drive systems, there are still two key issues to be solved. One issue is that there is serious voltage fluctuation on the DC-link, which increases the difficulty of suppressing the motor torque ripple and improving the grid current quality. Another issue is that even under steady operating conditions, there is always torque ripple due to the AC component in motor output power.

In this paper, a control strategy combined harmonic current injection and repetitive control (RC) is proposed to improve the dynamic performance and reduce the torque ripple. Different with existing control methods, harmonic current injection is used to reduce the different between the grid power and motor power. Therefore, the fluctuation voltage on the DC-link can be remarkably reduced even if motor output power can be kept stable. In addition, a modified RC is adopted in speed control loop to reduce the torque ripple under steady operating state and enhance the dynamic motor performance.

II. INFLUENCE OF DC-LINK VOLTAGE FLUCTUATION ON MOTOR PERFORMANCE

The SC motor drive system in this paper is composed of a diode rectifier, a PFC circuit and a motor inverter, as shown Fig.1. The PFC circuit is used to control the grid power, and the motor inverter is used to control the motor speed and torque.

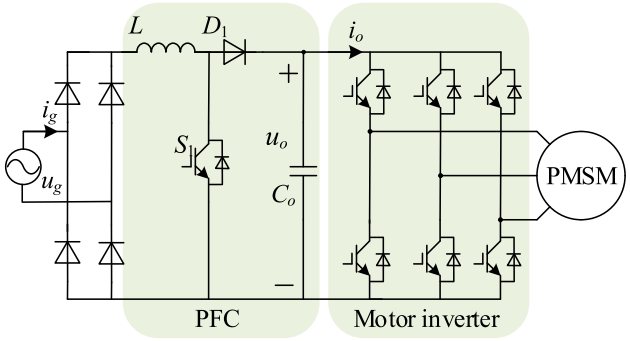

FIGURE 1. SC motor drive system based on boost FPC.

When the input PF is unity and the THD of the grid current is zero, the input power of motor drive systems can be expressed as

$$p_{in} = 2U_g I_g \sin^2(\omega t) = \frac{P_{in}}{P_M} - \frac{P_{in}\cos(2\omega t)}{p_r} \qquad (1)$$

where U_g and I_g are the RMS values of the grid voltage and current, respectively. ω is the angular frequency of the grid voltage, and p_{in}, P_{in}, and p_r are the input instantaneous power, the input average power, and the pulsating power of motor drive systems, respectively. The power curves of motor drive systems are plotted according to (1), as shown in Fig.2.

(1) and Fig.2 show the instantaneous grid power is composed of DC component and ripple component with twice grid frequency, and the DC power is equal to the motor power P_M. According to (1), the input power of motor drive

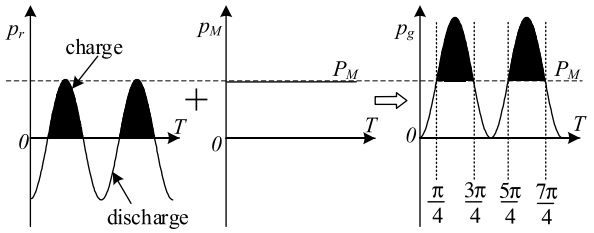

FIGURE 2. The power curves of motor drive systems.

systems can be obtained from the motor power.

$$p_g = 2P_M \sin^2(2\omega t) \tag{2}$$

(1) and (2) show that in motor drive systems powered by the grid, energy storage units are necessary to deal with p_r to achieve stable motor power. The power converter shown in Fig.1 has two energy storage devices: inductor L and capacitor C. Since the energy storage capacity of the capacitor is much higher than that of the inductor, it can be considered that p_r is totally deal with by C. When the power of C changes, the voltage of C is given as

$$\begin{aligned} W_r &= \int_{\pi/4(5\pi/4)}^{3\pi/4(7\pi/4)} (P_M \cos 2\omega t)dt \\ &= = \frac{1}{2}C(U_{cmax}^2 - U_{c\min}^2) = CU_C\Delta U\frac{P_M}{\omega} \end{aligned} \tag{3}$$

where U_{cmax} and U_{cmin} are the maximum voltage and the minimum voltage of the capacitor C in a quarter of the grid period. U_C and ΔU are the average voltage and the peak-peak voltage of the capacitor C, respectively. (3) shows ΔU increases with the decrease of the capacitor C. For SC motor drive systems, the capacitor C is only one-fifth to one-tenth of traditional motor drive systems, and ΔU will increase by 5-10 times. No doubt, there is serious voltage fluctuation on the DC-link.

The instantaneous power of the DC-link capacitor can be expressed as

$$p_c = i_c u_c = C\frac{du_c}{dt}u_c = p_r \tag{4}$$

Integrating both sides of (4) with respect to time, the capacitor voltages of C is expressed as

$$u_C = \sqrt{U_C^2 + \frac{P_M \sin(2\omega t)}{\omega C}} \tag{5}$$

where u_c and U_c are the instantaneous DC-link voltage and the average DC-link voltage of motor drive systems, respectively, and C is the capacitance of DC-link capacitor. Using $sin(2\omega t)$ as a variable to perform Taylor expansion, (5) can be simplified as

$$u_C \approx U_C + \frac{P_M}{2\omega CU_C}\sin(2\omega t) \tag{6}$$

(6) shows u_c is composed of the DC component U_c and the 2ω AC component. For SC motor drive systems, there is larger voltage fluctuation on the DC-link voltage due to the significant reduction of the capacitor C. Therefore, SC motor drive suffers from serious distortion of the grid current and motor torque.

For PMSM, the voltage of X phase windings is described as

$$u_X = \frac{u_c}{\sqrt{3}} = \frac{U_C + \frac{P_M}{2\omega CU_C}\sin(2\omega t)}{\sqrt{3}} \tag{7}$$

where X is any one of the three windings of PMSMs A, B and C. u_x is the voltage of X-phase winding.

Meanwhile, the voltage of X-phase winding is also expressed as

$$u_X = R_X i_X + L_X\frac{di_X}{dt} + E_0 \tag{8}$$

where R_X, i_X, and L_X are the winding resistance, the phase current, and the inductance, respectively. E_0 is the EMF of X-phase, which is constant under stable operating condition. (9) can be derived from (7) and (8)

$$\frac{U_C + \frac{P_M}{2\omega CU_C}\sin(2\omega t)}{\sqrt{3}} = R_X i_X + L_X\frac{di_X}{dt} + E_0 \tag{9}$$

(9) shows the current of X-phase has 2nd harmonic component, and the harmonic current increases with the increase of the AC component of the DC-link voltage. According to amplitude equivalent transformation, i_q also has the 2nd harmonic components, which results in torque ripple with the same frequency, as shown in Fig.3.

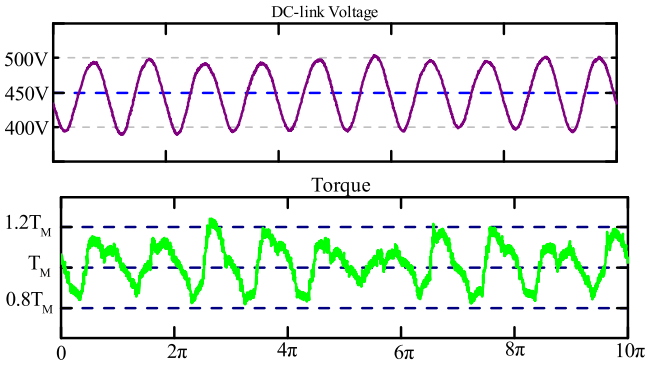

FIGURE 3. DC-link voltage and torque waveforms of SC drive systems based on traditional control.

III. HARMONIC INJECTION CONTROL STRATEGY

It is well known that p_r is the main reason to degrade the performance of SC motor drive systems. If p_r is reduced under the same P_M, smaller voltage fluctuations on the DC-link and smaller motor torque ripple can be achieved. The existing literatures show the 3rd injected harmonic current in phase with the grid voltage can effectively reduce p_r. (10) is the input power of SC motor drive systems with the 3rd injection harmonic current

$$p_{[1+3]in} = \frac{2U_g I_g \sin^2(\omega t)}{p_{1in}} + \frac{2kU_g I_g \sin(\omega t)\sin(3\omega t)}{p_{3in}} \tag{10}$$

where $p_{1\text{in}}$ and $p_{3\text{in}}$ are the input instantaneous power corresponding to the fundamental current and the 3rd harmonic current, respectively. $p_{[1+3]\text{in}}$ is the total input instantaneous power. k is the ratio of the 3rd harmonic current to the fundamental current and less than 1. (10) can be rewritten as

$$p_{[1+3]in} = \frac{P_{[1+3]in}}{\mathrm{P_M}} - \frac{P_{[1+3]in}\left[\frac{1-k}{2}\cos(2\omega t) + \frac{k}{2}\cos(4\omega t)\right]}{p_r} \tag{11}$$

where $\mathrm{P}_{[1+3]\text{in}}$ is the average input power and is equal to $\mathrm{P_M}$. (11) shows that $p_{[1+3]\text{in}}$ is composed of average power, ripple power with the 2nd harmonic and ripple power with the 4th harmonic. Substituting the p_r of (11) into (5), the DC-link voltage is rewritten as

$$u_c = \sqrt{U_c^2 + \frac{P_M}{2\omega C}\left[(1-k)\sin(2\omega t) + \frac{k}{2}\sin(4\omega t)\right]} \tag{12}$$

The DC-link voltage curves with different k are plotted according to (12), as shown in Fig.4. These curves show the fluctuation voltages on the DC-link decrease with the increase of the 3rd harmonic current. When k equals to 0.4, the fluctuation voltage will drop by 30%, which effectively suppresses the fluctuation voltage. But, the input PF and the THD become worse with the increase of k. Thus, k should be calculated carefully to meet the requirements of the input PF and the THD of SC motor drive systems.

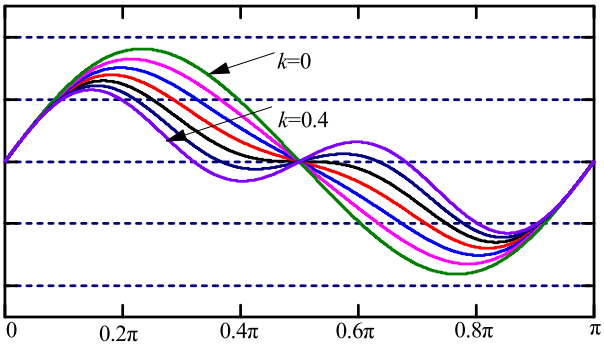

FIGURE 4. DC-link voltage with different 3rd injected harmonic current.

The input PF is given as

$$\mathrm{PF} = \frac{I_g}{\sqrt{I_g^2 + \left(kI_g^2\right)}} = \frac{1}{\sqrt{1+k^2}} \tag{13}$$

(13) shows the input PF is only related to k. For motor drive systems, the input PF should be greater than 0.9 under stable operating conditions. Then, the k should be less than 0.484. However, the 3rd harmonic current with the same k varies with different $\mathrm{P_M}$. When the motor power becomes higher, the 3rd harmonic current is no longer satisfy the IEC 61000-3-2 standard. Therefore, the k should be dynamically obtained according to motor power.

Fig.5 shows the resolve process of k. At first, the input PF is set as at least 0.95. And then, the 3rd harmonic currents are calculated according to (14)

$$I_{3in} = kI_g = \frac{2P_M}{U_g}\sqrt{\frac{1}{PF^2} - 1} \tag{14}$$

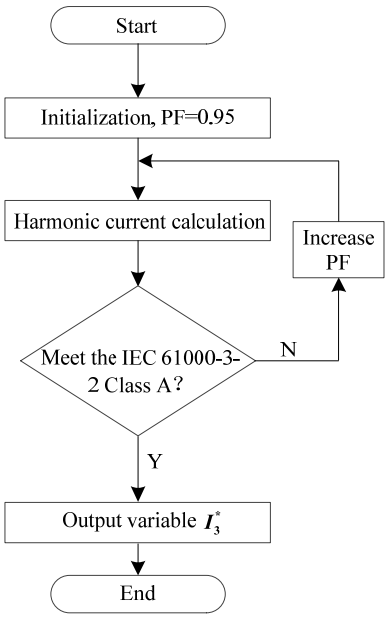

FIGURE 5. Flow chart of the parameter selection.

In IEC61000-3-2, the maximum value of the 3rd harmonic current should be less than 2.3A. If $I_{3\text{in}}$ is less than 2.3A, k should increase to reduce the voltage fluctuation on the DC-link. Meanwhile, the input PF should be greater than 0.9. In contrast, k should decrease to make the 3rd harmonic current satisfy the standard of IEC61000-3-2. When the motor power changes, the voltage fluctuation on the DC-link should be controlled within reasonable scope. k will be adjusted according to Fig.5. Then, the grid reference current i_g with injected 3rd harmonic current is:

$$i_g^* = \left|I_g \sin\omega_g t + kI_g \sin 3\omega_g t\right| \tag{15}$$

The above analysis shows that when the reasonable 3rd harmonic current is injected into SC motor drive systems, the voltage fluctuation on the DC-link can be greatly reduced, which improve the motor performance. Meanwhile, this system can still meet the current harmonic and input PF of IEC61000-3-2.

IV. COMBINED CONTROL STRATEGY BASED ON REPETITIVE CONTROL AND PI CONTROL

(12) and Fig.4 show there is voltage fluctuation on the DC-link even if the 3rd harmonic current is injected into SC motor drives. Due to the limitation of the traditional PI controller, it cannot suppress the motor torque ripple caused by the DC-link fluctuation voltage.

RC strategy can suppress motor torque ripple. However, this control has poor dynamic performance. In this section, a combined control strategy for SC motor drive systems is proposed. Under steady operating states, an improved RC strategy is adopted to suppress the torque ripple due to DC-link voltage fluctuation. Under dynamic operating states, a PI controller is introduced to increase the dynamic motor performance.

Both the DC-link voltage fluctuation and the inherent vibration of the motor will cause motor torque ripple. However, for SC motor drive systems, the DC-link voltage fluctuation is the main factor of motor torque ripple, so this paper only considers it. Since the motor torque and the DC-link voltage ripple frequency are both 100Hz, the resonant frequency of the repetitive controller is set to 100Hz. The bode diagram of the RC is describe as shown Fig.6. The diagram shows the RC has high gain at 100Hz, which can effectively suppress the disturbance of the AC component of the DC-link voltage to the motor torque.

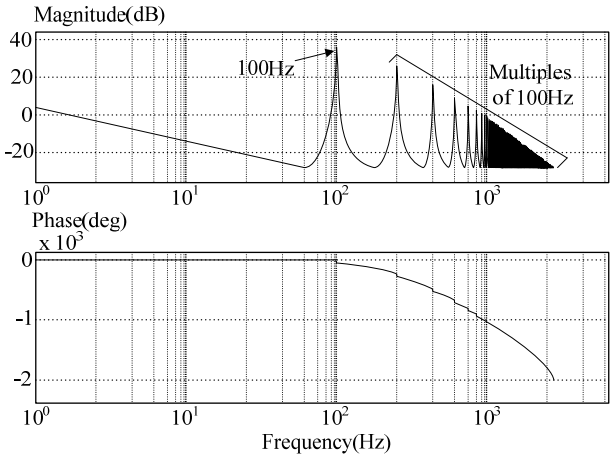

FIGURE 6. Bode diagram of the repetitive controller.

Fig.7 shows the block diagram of speed control. n^* is the given speed, and e(z) is the error between the given speed and the feedback speed. The discrete transfer function $G_{RC(z)}$ of repetitive controller can be expressed as

$$G_{RC}(z) = \frac{z^{-N+R}k_{RC}}{1 - Q(z)z^{-N}} \tag{16}$$

where N is the ratio of the sampling frequency of repetitive controller to the controlled object frequency. R is an advance link, which is used to compensate the phase delay. K_{RC} is the gain of the repetitive controller, which determine the error of system response time and the degree of stability. Q(z) is a low pass filter, which is used to enhance system stability and to improve the robustness of the closed-loop systems.

It can be seen from Fig.7 that the characteristic equation of the transfer function of speed error is

$$z^N - Q(z) + z^R k_{RC} = 0 \tag{17}$$

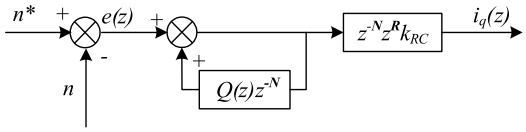

FIGURE 7. Speed controller with RC.

According to the stability conditions of the discrete system, the modulus of all the characteristic roots should be less than 1 ($|z_i| < 1$). It can be expressed as

$$z^N = \left| Q(z) - z^R k_{RC} \right| < 1 \tag{18}$$

For (18), the smaller the solution value, the greater the system stability margin. The N is selected as 200 according to the fluctuation frequency of DC-link voltage. Since Z^N will result in a phase lag at low frequencies, phase compensation should be adopted and R is selected as 5 according to the phase lag of the repetitive controller. For the low-pass filter Q(z), a constant 0.93 is selected as the filter in this paper after comprehensively considering the steady-state error and the stability of the system. The value of K_{RC} needs to take into account the stability margin and convergence speed of the system, and is selected as 0.7 according to the characteristic of SC motor drive systems.

When the load of SC motor drive systems suddenly changes, the output of repetitive controller will not change immediately due to delay characteristic of the repetitive controller. Thus, a combined with RC and PI control is adopt to improve the dynamic performance of SC motor drive systems, as shown in Fig.8.

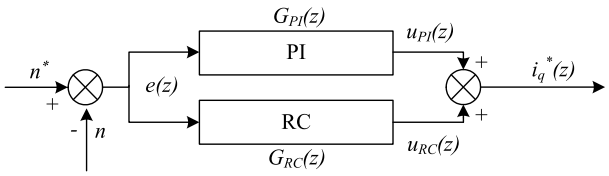

FIGURE 8. Speed controller with combined repetitive and PI control.

Under the combined controller, the given d-axis current can be expressed as

$$i_q^* = \left(\frac{z^{-N+R}k_{RC}}{1 - Q(z)z^{-N}}S(z) + G_{PI}(z)\right) \cdot (n^* - n) \tag{19}$$

Under steady operating states, SC motor drive systems have small speed error and small torque ripple with repetitive controller. Under dynamic operating states, the PI controller can quickly trace the error of speed and torque. Thus, the combined controller can effectively overcome the problems of dynamic response delay and torque ripple, and achieve a significant improvement in system steady-state and dynamic performance.

V. EXPERIMENTAL RESULTS

To verify the proposed combined control method, a test platform is been built, which is shown in Fig.9, and the key parameters of the SC motor drive system are

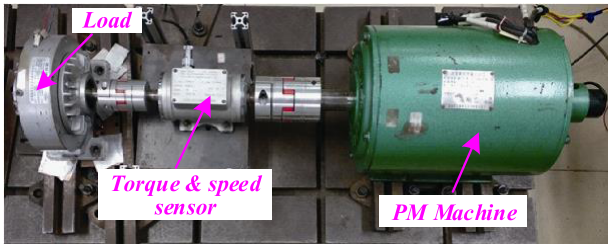

FIGURE 9. Experimental platform setup.

TABLE 1. Key parameters of the SC motor drive.

Parameters	Value
U_g	220 V
ω	314 rad/s
Power switching frequency	20 kHz
C_o	100μF
U_o and U	450/150

TABLE 2. Key parameters of the test motor.

Parameters	Value
Rated power	0.4 kW
Rated torque	3N·m
Rated torque	1500 rpm
Pole,*P*	4

listed in Table 1. The average DC-link voltage is selected as 400V, and the peak-peak voltage of DC-link is 50V. The FS30R06W1E3 IGBT module of Infineon Technologies is employed to drive the motor. The control scheme is implemented using TMS320F28335 DSP, which generates the control logic of PFC and motor inverter.

In the SC motor drive system, only a 100μF film capacitor is adopted. In traditional motor drive system, a 680 μF electrolytic capacitor is adopted to obtain the same ripple voltage on the DC-link, which is more than 6 times the SC motor drive system in this paper.

Fig.10 shows the overall diagram of the proposed control strategy for SC motor drive systems. There are two control goals: small DC-link fluctuation voltage and high motor performance. For the first goal, the 3rd injected harmonic current is calculated according to (13) and (14), and the feedback gird current is obtained by current Hall sensor. Then, S is turned on or off according to the error between the reference i_g^* and the feedback i_g.

For motor control, SVPWM with $id = 0$ is adopted. The motor speed n and the rotor position are obtained by a photoelectric encoder. The output of the speed controller is the current reference iq^* according to the error between the given speed n^* and the feedback speed n. Different with traditional motor controller, the combined controller based on PI and RC is adopted in this paper. The feedback id and iq are obtained by abc-dq coordinate transformation. The current controller obtains u_d and u_q based on the error between the reference iq^* and the feedback iq, 0 and the feedback

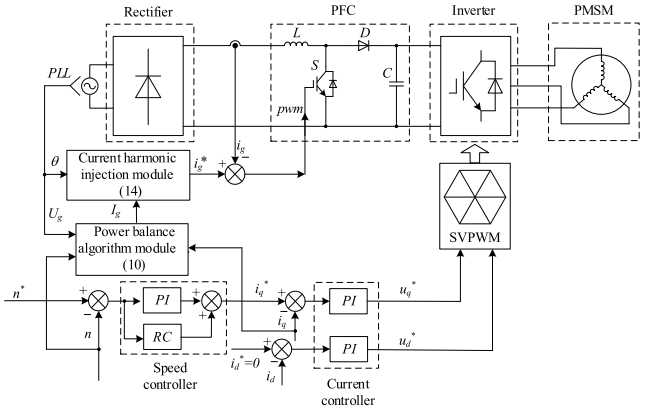

FIGURE 10. Overall diagram of SC motor drive systems.

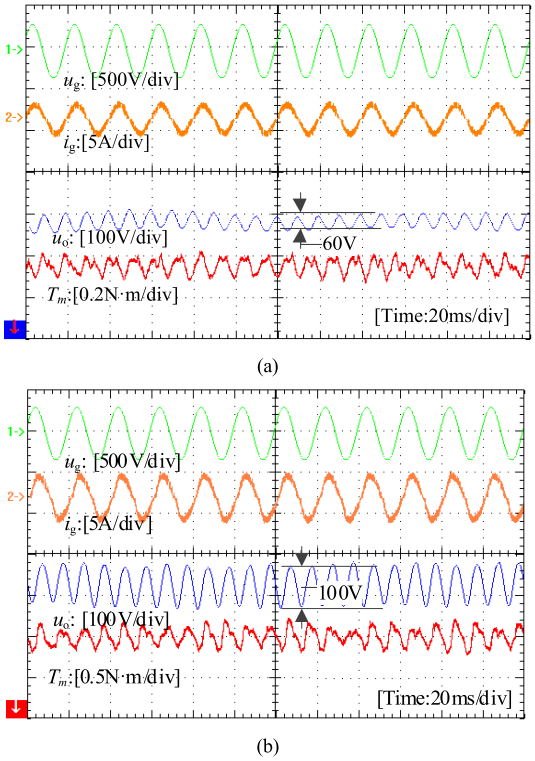

FIGURE 11. Experimental waveforms of SC motor drive system based on traditional control. (a) n = 1000rpm, TL = 1 N·m. (b) n = 1000rpm, TL = 2 N·m.

current id, respectively. And then, the control signal of the motor inverter is generated by SVPWM control to realize the high-performance operation of the PMSM.

Two experiments are performed to evaluate the performance of the combined control. In the first experiment, only 3rd injected harmonic current is test, and motor drive system is still controlled by traditional PI controller. In the second experiment, the combined control based RC and PI is verified under steady and dynamic operating conditions.

In the first experimental, the given speed n is 1500rpm, and the load T_L is 1N·m and 2 N·m, respectively. Fig.11 and Fig.12 show the DC-link voltage experimental waveforms of SC motor drive system under the traditional control and 3rd injected harmonic current control, respectively.

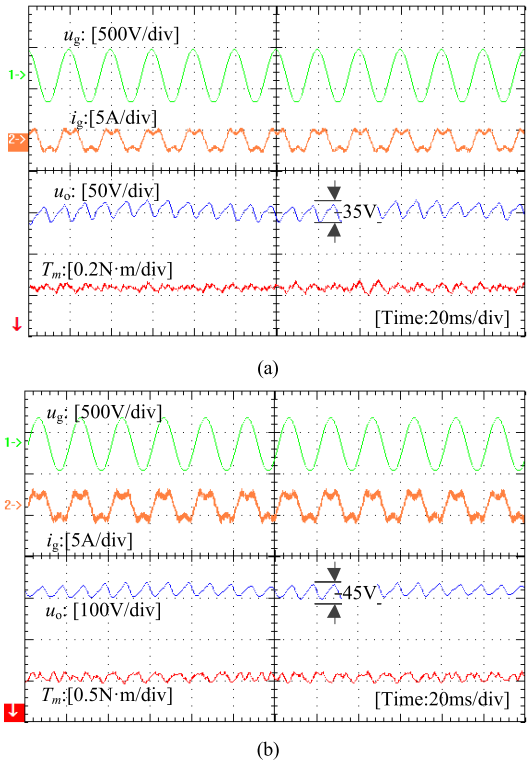

FIGURE 12. Experimental waveforms of SC motor drive system based on 3rd injected harmonic current. (a) n = 1000rpm, TL = 1 N·m. (b) n = 1000rpm, TL = 2 N·m.

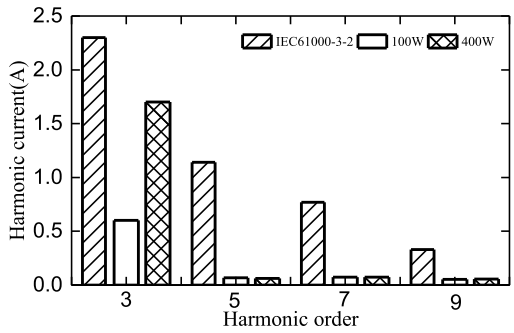

FIGURE 13. Experimental waveforms of SC motor drive system based on 3rd injected harmonic current.

The results show the fluctuation voltage on the DC-link under the two operating conditions reduce by 41% and 55% when 3rd harmonic current is injected, which shows the injected harmonic current can effectively suppress the fluctuation voltage on the DC-link. Fig.13 shows the harmonic currents of SC motor drive system with 100W and 400W when 3rd harmonic current is injected, which can satisfy the harmonic standard of IEC61000-3-2. In addition, it can be seen from Fig.12 that although the motor torque ripples under the two operating conditions are reduced by 20% and 25%, respectively, there is periodic torque ripple due to voltage fluctuation on the DC-link.

In the second experiment, RC is applied in SC motor drive system to furtherly suppress the torque ripple. Fig.14 shows

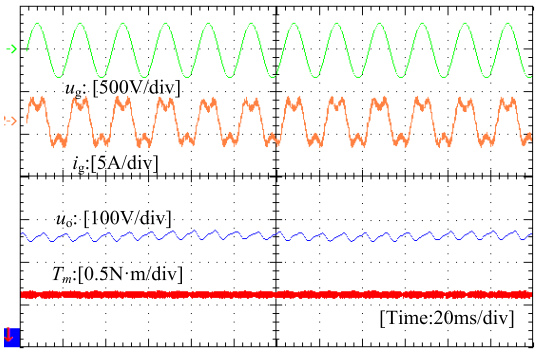

FIGURE 14. Experimental waveforms of SC motor drive system based on RC.

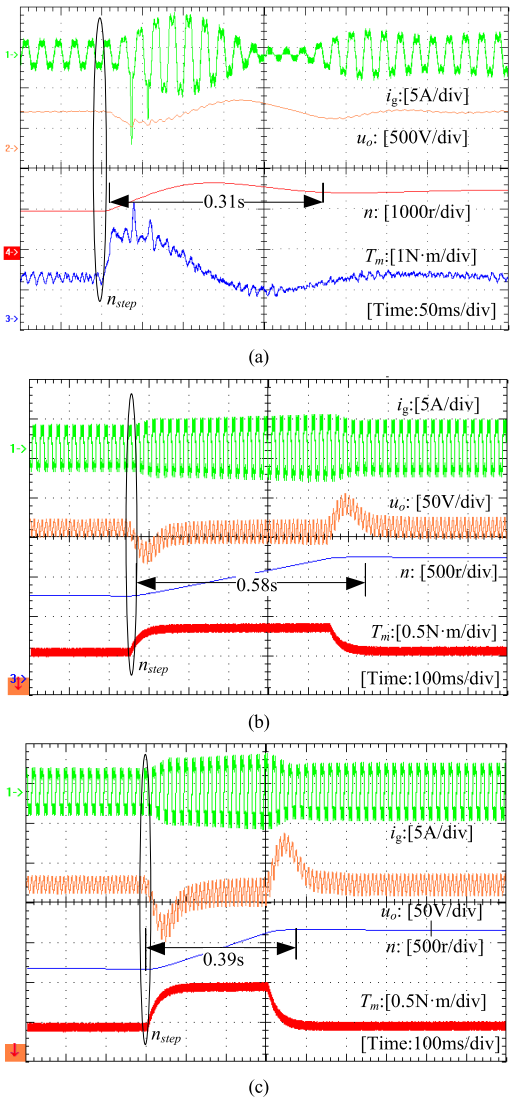

FIGURE 15. Dynamic experimental waveforms of SC motor drives with speed-up from 1000 to 1500rpm. (a) PI control. (b) Only RC. (c) PI + RC.

the experimental waveforms of SC motor drive system under steady operating condition based on RC. The given speed n is 1500rpm, and the load T_L is 2 N·m. The torque ripple is 0.1N·m based on RC under steady operating

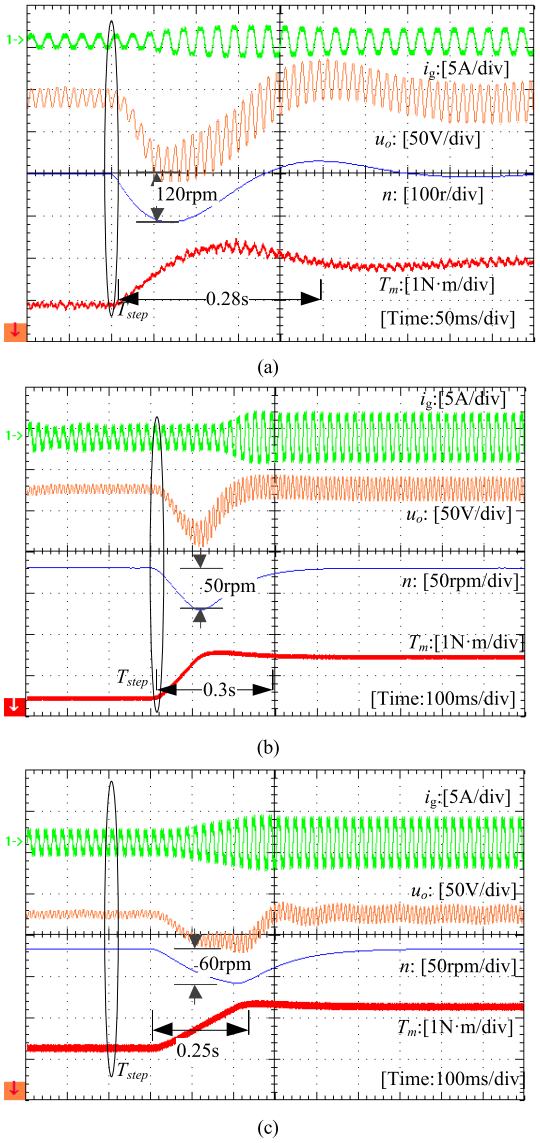

FIGURE 16. Dynamic experimental waveforms of SC motor drives with load-up from 1 to 2N·m. (a) PI control. (b) Only RC. (c) PI + RC.

condition, which is significantly lower than the motor torque ripple based on PI control.

Fig.15 shows the experimental waveforms of SC motor drive system at variable speed working conditions with the 2N·m load. At the time n_{step}, a step change in the given speed happen from 1000 to 1500rpm. Although the torque ripple of the SC motor drive system is effectively suppressed based on RC, the dynamic speed response performance of the repetitive controller is significantly lower than that of the traditional PI control drive when the given speed changes suddenly, as shown in Fig.15 (a) and (b). It can be known form experimental waveforms based on RC that the actual speed reaches the reference one and maintains with a small ripple within 0.58s, which is about 2 times that of the traditional PI controller. When the combined RC and PI control is applied in the SC motor drive system, it takes 0.38s to reach the given speed again, which is close to the PI control. Meanwhile, the torque ripple is greatly reduced. Thus, the combined RC and PI control has better performance of the SC motor drive system than traditional PI control and RC for speed-up operating conditions.

Fig.16 shows the experimental waveforms of SC motor drive system at variable load working conditions with 1000rpm. At the time T_{step}, a step-up load happens from 1 to 2 N·m. These experiments have the same PI controller parameters. It can be seen from Fig.16 there are basically the same DC-link voltage drop and motor speed drop in three experiments. Although the traditional PI control has the shortest adjust time when the step-up load happens, there is obvious overshoot torque, which degrades the dynamic performance of the SC motor drive system. In addition, the torque ripple is larger than other control methods. Fig.16(b) shows that RC has the shortest adjustment time in three control methods due to the characteristic of RC. Fig.16 (c) shows that when PI control is combined with RC, the SC motor drive system has better dynamic performance within small torque ripple.

VI. CONCLUSION

This paper has proposed a hybrid control strategy, which can improve the dynamic performance and suppress the torque ripple of SC motor drive systems. To suppress the DC-link voltage fluctuation, the 3$^{\text{rd}}$ injected harmonic current control method is applied in SC motor drive systems. The guideline of injected harmonic current is deduced to satisfy the standard of IEC61000-3-2 and high input PF. In addition, a combined RC and PI control is proposed. In this combined controller, RC is used to suppress the torque ripple because there is periodic DC-link voltage ripple. And the PI control is used to improve the dynamic performance of SC motor drive system. Compared with the conventional control methods, the proposed hybrid control strategy has better dynamic performance and lower torque ripple, which is important for SC motor drive systems. The prototype experiments showed that the proposed control method is effective under steady-state and dynamic operating conditions.

REFERENCES

[1] X. Zhu, Z. Xiang, C. Zhang, L. Quan, Y. Du, and W. Gu, "Co-reduction of torque ripple for outer rotor flux-switching PM motor using systematic multi-level design and control schemes," *IEEE Trans. Ind. Electron.*, vol. 64, no. 2, pp. 1102–1112, Feb. 2017.

[2] H. Wang and F. Blaabjerg, "Reliability of capacitors for DC-link applications in power electronic converters—An overview," *IEEE Trans. Ind. Appl.*, vol. 50, no. 5, pp. 3569–3578, Oct. 2014.

[3] G. M. Buiatti, S. M. A. Cruz, and A. J. M. Cardoso, "Lifetime of film capacitors in single-phase regenerative induction motor drives," in *Proc. IEEE Int. Symp. Diag. Electr. Mach., Power Electron. Drives*, Sep. 2007, pp. 356–362.

[4] X. Cao, Q.-C. Zhong, and W.-L. Ming, "Ripple eliminator to smooth DC-bus voltage and reduce the total capacitance required," *IEEE Trans. Ind. Electron.*, vol. 62, no. 4, pp. 2224–2235, Apr. 2015.

[5] *Electromagnetic Compatibility (EMC): Limits-Limits for Harmonic Current Emissions*, Standard IEC 61000-3-2, Part 3-2, 2005.

[6] W. Yao, P. C. Loh, Y. Tang, X. Wang, X. Zhang, and F. Blaabjerg, "A robust DC-split-capacitor power decoupling scheme for single-phase converter," *IEEE Trans. Power Electron.*, vol. 32, no. 11, pp. 8419–8433, Nov. 2017.

[7] C. Zhang, L. Xu, X. Zhu, Y. Du, and L. Quan, "Elimination of DC-link voltage ripple in PMSM drives with a DC-split-capacitor converter," *IEEE Trans. Power Electron.*, vol. 36, no. 7, pp. 8141–8154, Jul. 2021.
[8] Y. Tang, Z. Qin, F. Blaabjerg, and P. C. Loh, "A dual voltage control strategy for single-phase PWM converters with power decoupling function," *IEEE Trans. Power Electron.*, vol. 30, no. 12, pp. 7060–7071, Dec. 2015.
[9] Y. Son and J.-I. Ha, "Direct power control of a three-phase inverter for grid input current shaping of a single-phase diode rectifier with a small DC-link capacitor," *IEEE Trans. Power Electron.*, vol. 30, no. 7, pp. 3794–3803, Jul. 2015.
[10] H. Lamsahel and P. Mutschler, "Permanent magnet drives with reduced DC-link capacitor for home appliances," in *Proc. 35th Annu. Conf. IEEE Ind. Electron. (IECON)*, Nov. 2009, pp. 725–730.
[11] J. C. W. Lam and P. K. Jain, "A high power factor, electrolytic capacitorless AC-input LED driver topology with high frequency pulsating output current," *IEEE Trans. Power Electron.*, vol. 30, no. 2, pp. 943–955, Feb. 2015.
[12] K. Inazuma, H. Utsugi, K. Ohishi, and H. Haga, "High-power-factor single-phase diode rectifier driven by repetitively controlled IPM motor," *IEEE Trans. Ind. Electron.*, vol. 60, no. 10, pp. 4427–4437, Oct. 2013.
[13] S. Kim and J.-K. Seok, "Induction motor control with a small DC-link capacitor inverter fed by three-phase diode front-end rectifiers," *IEEE Trans. Power Electron.*, vol. 30, no. 5, pp. 2713–2720, May 2015.
[14] B. Kwak, J.-H. Um, and J.-K. Seok, "Direct active and reactive power control of three-phase inverter for AC motor drives with small DC-link capacitors fed by single-phase diode rectifier," *IEEE Trans. Ind. Appl.*, vol. 55, no. 4, pp. 3842–3850, Jul. 2019.
[15] Y. Feng, L. Mathe, K. Lu, F. Blaabjerg, X. Wang, and P. Davari, "Analysis of harmonics suppression by active damping control on multi slim DC-link drives," in *Proc. IECON 42nd Annu. Conf. IEEE Ind. Electron. Soc.*, Oct. 2016, pp. 5001–5006.
[16] K. Abe, Y. Akama, K. Ohishi, H. Haga, and Y. Yokokura, "Suppression method of increase in motor current at zero output voltage for an electrolytic capacitor-less inverter," in *Proc. IEEE Int. Conf. Ind. Electron. Sustain. Energy Syst. (IESES)*, Jan. 2018, pp. 168–173.
[17] M. Cespedes, L. Xing, and J. Sun, "Constant-power load system stabilization by passive damping," *IEEE Trans. Power Electron.*, vol. 26, no. 7, pp. 1832–1836, Jul. 2011.
[18] N. Zhao, G. Wang, D. Xu, and D. Xiao, "An active damping control method for reduced DC-link capacitance IPMSM drives," *IEEE Trans. Ind. Electron.*, vol. 65, no. 3, pp. 2057–2068, Mar. 2018.
[19] K. Abe, H. Haga, K. Ohishi, and Y. Yokokura, "Fine current harmonics reduction method for electrolytic capacitor-less and inductor-less inverter based on motor torque control and fast voltage feedforward control for IPMSM," *IEEE Trans. Ind. Electron.*, vol. 64, no. 2, pp. 1071–1080, Feb. 2017.
[20] J.-H. Jung, H.-J. Heo, J.-M. Kim, and S.-U. Choi, "DC-link voltage stabilization and source THD improvement using d-axis current injection in reduced DC-link capacitor system," in *Proc. IECON 42nd Annu. Conf. IEEE Ind. Electron. Soc.*, Oct. 2016, pp. 2737–2742.
[21] W.-J. Lee and S.-K. Sul, "DC-link voltage stabilization for reduced DC-link capacitor inverter," in *Proc. IEEE Energy Convers. Congr. Expo.*, Sep. 2009, pp. 1740–1744.
[22] H.-S. Jung, S.-J. Chee, S.-K. Sul, Y.-J. Park, H.-S. Park, and W.-K. Kim, "Control of three-phase inverter for AC motor drive with small DC-link capacitor fed by single-phase AC source," *IEEE Trans. Ind. Appl.*, vol. 50, no. 2, pp. 1074–1081, Mar. 2014.
[23] N. Zhao, G. Wang, D. Xu, L. Zhu, G. Zhang, and J. Huo, "Inverter power control based on DC-link voltage regulation for IPMSM drives without electrolytic capacitors," *IEEE Trans. Power Electron.*, vol. 33, no. 1, pp. 558–571, Jan. 2018.

CHAO ZHANG (Member, IEEE) received the M.Sc. degree in control theory and control engineering from the China University of Mining and Technology, Xuzhou, China, in 2001, and the Ph.D. degree in electrical engineering from Zhejiang University, Hangzhou, China, in 2006.

He has been with Jiangsu University, since 2006, where he is currently an Associate Professor with the School of Electrical and Information Engineering. His research interests include small capacitor drive systems, high performance control of permanent magnet motors, and renewable energy.

LEI XU (Member, IEEE) received the B.Sc. degree in electrical engineering and automation from the Yancheng Institute of Technology, Yancheng, China, in 2010, the M.Sc. degree in electrical engineering from Jiangsu University, Zhenjiang, in 2013, and the Ph.D. degree in electrical engineering from Southeast University, Nanjing, in 2017.

He is currently a Lecturer with the School of Electrical and Information Engineering, Jiangsu University. His current research interests include the high-performance permanent magnet motors, linear and rotary permanent magnet motors, renewable energy generation systems, and intelligent manufacturing equipment's drive.

XIAOYONG ZHU (Member, IEEE) received the B.Sc. and M.Sc. degrees from Jiangsu University, Zhenjiang, China, in 1997 and 2002, respectively, and the Ph.D. degree from the School of Electrical Engineering, Southeast University, Nanjing, China, in 2008, all in electrical engineering.

He has been with Jiangsu University, since 1997, where he is currently a Professor with the School of Electrical Information Engineering. From 2007 to 2008, he was a Research Assistant with the Department of Electrical and Electronic Engineering, University of Hong Kong. From 2012 to 2013, he was a Visiting Professor with the Graduate Automotive Technology Education Center for Electric Drive Transportation, University of Michigan, Dearborn, MI, USA, funded by the Department of Energy. His current research interests include design and drive control of electric machines with wide-speed range, less rare-earth permanent-magnet motors, and multiport permanent-magnet motors.

YI DU (Member, IEEE) received the B.Sc. and M.Sc. degrees in electrical engineering from Jiangsu University, Zhenjiang, China, in 2002 and 2007, respectively, and the Ph.D. degree in electrical engineering from Southeast University, Nanjing, China, in 2014.

He has been with Jiangsu University, since 2002, where he is currently a Professor with the School of Electrical and Information Engineering. His research interests include design and analyze electric machine system with low speed and high torque output, and with wide-speed range.

LI QUAN received the B.Sc. degree in electric machines and electric apparatus from the Hefei University of Technology, Hefei, China, in 1985, the M.Sc. degree in electric machines and electric apparatus from Southeast University, Nanjing, China, in 1991, and the Ph.D. degree in power electronics and power transmission from the Nanjing University of Aeronautics and Astronautics, Jiangsu, China, in 2007. Since 1998, he has been with Jiangsu University, Zhenjiang, China, where he is currently a Professor with the School of Electrical and Information Engineering. He has authored or coauthored more than 100 technical articles, one textbook, and holds three patents in these areas. His teaching and research interests include high-performance permanent magnet motors for electric vehicles, double rotor permanent-magnet motors for hybrid electric vehicles, and motor drive control.